MMUST PUBLISHING PRESS

Journal of Advances in Science, Engineering and Technology

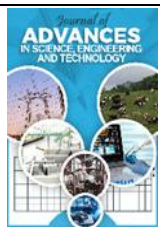

Ionospheric Response to Intense Geomagnetic Storms of 17 March 2015 and 22 June 2015 over the East African region

Wilberforce Muniafu[a*], Boniface Ndinya[a], George Omondi[b]

[a]*Department of Physics, School of Natural Sciences, Masinde Muliro University of Science and Technology, Kakamega, Kenya.*

[b]*Department of Physics and Materials Science, Maseno University, Maseno, Kenya.*

ABSTRACT

The variation of Total Electron Content (TEC) derived from seven International Global Navigation Satellite System (GNSS) stations (IGS) over the East African low latitude region for intense geomagnetic storms of 17 March 2015 and 22 June 2015 was investigated. The O/N2 maps were accessed from the GUVI website. Daily variation of Dst, IMF Bz, IEF Ey, and solar wind speed for the period was analyzed. The results showed during the storm of 17 March 2015 a positive storm effect was noticed over the station during the initial and main phase of the storm across the stations which was attributed to the prompt penetration of high-latitude electric fields to lower latitudes and the effect of Equatorial Ionization Anomaly (EIA) and negative storm effect which was attributed to the downward E × B drift and depletion of O/N2 over the East African region. During the storm of 22 June 2015, there was a positive storm effect during the recovery period across all the stations, which was also attributed to the prompt penetration of high-latitude electric fields to lower latitudes and the effect of EIA. The study also revealed that the storm impacts varied with local time and season, with greater effects during the equinox period, indicating that local time plays a role in the ionospheric response to geomagnetic storms.

ARTICLE INFO

Keywords:
Geomagnetic storm,
Total electron content,
Prompt penetration electric field,
Disturbance dynamo electric field.

Article History:
Received 3 June 2025
Received in revised form 1 September 2025
Accepted 8 September 2025
Available online 14 October 2025

1. Introduction

The ionosphere plays a critical role in the propagation of trans-ionospheric radio waves, thereby influencing the performance of navigation systems and satellite-based communications (Ngwira et al., 2013). Under normal conditions, it is often considered as a continuous layer with a relatively smooth and uniform plasma density distribution. However, during disturbed periods, perturbations can induce localized plasma structuring, resulting in ionospheric electron density irregularities. Such irregularities contribute to signal degradation, including amplitude fading and phase scintillation, particularly in L-band frequencies used by Global Navigation Satellite Systems (GNSS) (Kintner et al., 2007).

Geomagnetic disturbances are a primary driver of Equatorial Plasma Bubbles (EPBs)—plasma irregularities characterized by depleted electron density relative to the background ionosphere (Carmo et al., 2024). These disturbances arise from fluctuations in the Interplanetary Magnetic Field (IMF) and manifest as geomagnetic storms, which generate large-scale perturbations in the Earth's magnetosphere (Pokharia, 2018). The associated storm-time electric fields, notably the Prompt Penetration Electric Field (PPEF) and the Disturbance Dynamo Electric Field (DDEF), play a significant role in controlling the initiation, development, and suppression of EPBs (Abdu, 2009; Carmo et al., 2009).

Geomagnetic storms also modulate the ionosphere by altering the Total Electron Content (TEC), which represents the total number of electrons contained in a column of unit cross-sectional area extending along the signal path between a Global Positioning System GPS satellite and a ground receiver (Adewale et al., 2012). Storm effects on TEC can manifest as either enhancements or depletions (Olwendo et al., 2015). An increase in electron density (positive storm effect) is commonly associated with the intensification of the equatorial fountain, driven by eastward PPEF

* Corresponding author. e-mail: muniafuw@gmail.com
Editor: Victor Odari, Masinde Muliro University of Science and Technology, Kenya.
Citation: Muniafu W., Ndinya B., & Omondi G. (2025). Ionospheric Response to Intense Geomagnetic Storms of 17 March 2015 and 22 June 2015 over the East African region. Journal of Advances in Science, Engineering and Technology 2(1), 26 – 35.

enhancement, as well as the action of equatorward neutral winds that suppress plasma diffusion and recombination processes (Lissa et al., 2020). Conversely, a reduction in electron density (negative storm effect) is linked to storm-induced decreases in the thermospheric O/N_2 ratio at low latitudes, reflecting compositional changes in the neutral atmosphere (Huang et al., 2005).

Ionospheric irregularities, defined as random spatial and temporal fluctuations in plasma density that modify the refractive index of the ionosphere, are notably enhanced during geomagnetic storms and substorms (Watson et al., 2011). Severe geomagnetic activity produces strong plasma irregularities, resulting in adverse impacts on satellite navigation accuracy, radar performance, and overall reliability of trans-ionospheric communication links (Kintner et al., 2007).

The ionospheric response to the geomagnetic storms of 17 March 2017 and 22 June 2015 over the Wuhan region, investigated using a GNSS-based tomographic technique, revealed that the observed negative storm effects were primarily driven by mechanisms such as the Disturbance Dynamo Electric Field (DDEF), Prompt Penetration Electric Field (PPEF), and neutral composition changes originating from high latitudes (Feng et al., 2021). Similarly, Uluma et al. (2019) analysed the variability of the Vertical Total Electron Content (VTEC) gradient and the TEC Rate Index (ROTI) over Kisumu, Kenya, during selected quiet and storm days in 2013 and 2014. Their analysis utilized RINEX data archived in the Scintillation Index Decision Aid (SCINDA) system at Maseno University. The findings indicated that ionospheric irregularities predominantly developed during post-sunset hours on both quiet and disturbed days, with greater intensity during geomagnetically active periods.

Chukwuma et al. (2022) examined ionospheric irregularities across Africa associated with TEC anomalies under high solar activity conditions. Using GNSS observations from AFREF stations distributed across low-latitude sites (MAL2, NKLG, CLBR) and mid-latitude sites (HRAO, SUTH, VACS), they reported that post-sunset ROTI values exceeded 1 TECU/min at low-latitude stations but remained below 1 TECU/min at mid-latitudes. However, this study included only a single station from the East African region, highlighting the need for additional investigations across the wider equatorial East African region.

Further contributions were made by Aol et al. (2019), who explored space weather effects on the ionosphere, and by Ondede et al. (2022), who investigated the relationship between geomagnetic storms and the occurrence of ionospheric irregularities over West Africa during the peak of solar cycle 24. Their study, which relied on data from seven GNSS stations in Nigeria (ABUZ, CLBR, FPNO, GEMB, HUKP, OCGF, UNEC), found only a weak correlation between Dst indices and irregularity parameters, implying that ionospheric irregularities are not exclusively controlled by geomagnetic storms. A separate investigation using GNSS data from five stations (NKLG, MBAR, MOIU, MAL2, SEYI) for the 17–28 February 2014 storm sequence revealed a delayed positive ionospheric response to the 19 February 2014 storm, attributed to neutral composition changes, while the recovery phase of the 20 February 2014 storm was marked by a negative storm effect driven by DDEF.

Habyarimana et al. (2023) conducted a comparative study of ionospheric storm-time effects over the East African sector during the 17 March storms of 2013 and 2015 within solar cycle 24, aiming to assess similarities and differences given their occurrence within the same seasonal window. In a related investigation, Muniafu et al. (2024) and Uluma et al, (2025) analysed the ionospheric TEC response to the intense geomagnetic storm of 10–11 May 2024 using data from six GNSS stations distributed across low-, mid-, and high-latitude regions. Their results indicated that stations located in the equatorial sector, particularly MBAR and BELE, exhibited enhanced VTEC values, attributed to the effects of PPEF. However, this study was limited by its reliance on a single storm event and one East African station (MBAR), underscoring the need for broader analyses incorporating multiple storms and additional International GNSS Service (IGS) stations within the region.

While many studies have investigated ionospheric responses to geomagnetic storms worldwide (e.g., Fuller-Rowell et al., 1994; Huang et al., 2005; Watson et al., 2011; Amaechi et al., 2018), the East African equatorial sector has received limited attention. Most existing research has concentrated on the American, Asian, and West African regions, where data availability is comparatively richer. In contrast, East Africa is characterized by distinctive electrodynamics and thermospheric features, including: its location near the geomagnetic equator and the Equatorial Ionization Anomaly (EIA) crests, pronounced seasonal differences between equinox and solstice responses, limited GNSS observational coverage, which constrains detailed storm-time analysis, and complex interactions between prompt penetration electric fields (PPEFs) and disturbance dynamo electric fields (DDEFs), which remain insufficiently quantified.

As a result, a significant knowledge gap persists in understanding how storm-time electrodynamics, thermospheric composition changes (O/N_2), and local time/seasonal effects collectively influence TEC over East Africa. Filling this gap is crucial for improving GNSS reliability and advancing space weather forecasting in a region particularly susceptible to ionospheric disturbances.

In the present work, the ionospheric response to two intense geomagnetic storms, namely those of 17 March 2015 and 22 June 2015, is investigated over the East African sector using dual-frequency GPS observations from six IGS stations: Malindi (Kenya), Eldoret (Kenya), Mbarara (Uganda), Addis Ababa (Ethiopia), Dodoma (Tanzania), and Mbeya (Tanzania)

2. Materials and Methods

The data for two days before and after the intense geomagnetic storms of 17 March 2015 and 22 June 2015 were considered in this research.

The variation of geomagnetic and interplanetary parameters including the Disturbance Storm Time index (Dst, nT), the southward component of the Interplanetary Magnetic Field (IMF Bz, nT), the dawn-dusk component of the Interplanetary Electric Field (IEF-Ey, mV m^{-1}), and solar wind speed (km s^{-1}) for the intervals 15–19 March 2015 and 20–24 June 2015 was obtained from the NASA OMNIWeb database. (https://omniweb.gsfc.nasa.gov/form/dx1.html). Global maps of the thermospheric composition ratio (O/N_2) for the same periods were retrieved from the TIMED/Global Ultraviolet Imager (GUVI) database (https://guvitimed.jhuapl.edu/guvi-galleryl3on2).

Ionospheric GPS data were collected from seven International GNSS Service (IGS) stations located within the East African region: Table 1 gives the geographic and geomagnetic coordinates of stations used in this study.

Table 1: The geographic and geomagnetic coordinates of stations used in this study.

City	Geographic coordinates		Geomagnetic coordinates	
Addis Ababa (ADIS)	9.04°N	38.77°E	~0.19°N	~111.1°E
Arusha (ARSH)	3.38°S	36.69°E	~ − 5.91°N	~110.5°E
Dodoma (DODM)	6.19°S	35.75°E	~ − 8.69°N	~109.7°E
Eldoret (MOIU)	0.29°N	35.29°E	~ − 2.76°N	~108.7°E
Malindi (MAL2)	2.99°S	40.19°E	~ − 5.32°N	~112.6°E
Mbarara (MBAR)	0.61°S	30.65°E	~ − 3.51°N	~105.2°E
Mbeya (MBEY)	9.03°S	33.43°E	~ − 11.68°N	~106.8°E

The data covering the intervals 15–19 March 2015 and 20–24 June 2015 were downloaded from the Crustal Dynamics Data Information System (CDDIS) archive (https://cddis.gsfc.nasa.gov/gps/data).

The GPS data were subsequently processed into Total Electron Content (TEC) using the GPS-TEC analysis software developed at the Institute for Scientific Research, Boston College, by Gopi Krishna Seemala (Seemala & Valladares, 2011). This software applies dual-frequency phase and code observations from L1 and L2 GPS signals to mitigate satellite and receiver clock biases as well as tropospheric water vapor effects, thereby enabling accurate computation of slant TEC (STEC in Eq. 1, where f_1 and f_2 are GPS satellite frequencies and p_1 and p_2 are differential code) (Sardon & Zarraoa, 1997; Sardon et al., 1994; Arikan et al., 2008).

$$STEC = \frac{1}{40.3}\left[\frac{f_1^2 f_2^2}{f_1^2 - f_2^2}\right](p_1 - p_2) \qquad (1)$$

The STEC values can be converted to Vertical TEC (VTEC) by spherical harmonics mapping function at the Ionospheric pierce point according to Eq. 2.

$$VTEC = STEC \times \cos\chi \qquad (2)$$

The zenith angle (χ) is given by Eq. 3, where θ is the satellite's elevation angle (in degrees). R_E denotes the Earth's radius, which is 6,378.137 km, and h is the height of the ionospheric layer, assumed to be 350 km based on Klobuchar (1987).

$$\chi = arcsin\left[\frac{R_E \cos\theta}{R_E + h}\right] \qquad (3)$$

To assess the impact of geomagnetic storms on ionospheric TEC, the mean TEC was computed from five geomagnetically quiet days within the same month. The percentage variation in TEC was subsequently determined using Eq. 4 (Tilahum et al, 2025).

$$\Delta TEC = \frac{TEC - TEC_q}{TEC_q} \times 100\% \qquad (4)$$

3. Results and Discussion

3.1. Variations of solar wind parameters.

Fig. 1 and Fig. 2 show the variation of Dst, IMF Bz, IEF Ey, and solar wind speed between 15 and 19 March 2015, 20 and 24 June 2015, respectively.

In Fig. 1(a), it is evident that during 15–16 March 2015, the Dst index remained relatively quiet with values below −20 nT. Similarly, in Fig. 2(a), during the pre-storm interval of 20–21 June 2015, the Dst index varied between 0 and −10 nT, indicating quiet geomagnetic conditions. Fig. 1(b-d) further illustrates that, during the pre-storm phase in March, the IMF Bz exhibited small oscillations northward and southward with magnitudes less than ± 10 nT. These fluctuations corresponded with variations in the interplanetary electric field (IEF Ey) within the range of approximately −5 to +5 mV m^{-1} and were accompanied by relatively low solar wind speeds, remaining below 450 km s^{-1}. Likewise, Figures 2(b-d) show that on 20–21 June 2015, the IMF Bz remained close to 0 nT, corresponding to near-zero IEF Ey values and low solar wind speeds ranging between 250–320 km s^{-1}.

On 17 March 2015, at approximately 03:00 UT, the sudden storm commencement (SSC) was observed, marked by an increase in solar wind speed and a northward turning of the IMF Bz to $\sim +13$ nT. This was associated with an IEF Ey of ~ 9 mV/m. Subsequently, the main phase of the storm was reached around 22:45 UT, when the Dst index recorded a minimum of −229 nT. This strong depression was associated with a pronounced southward turning of the IMF Bz to −24 nT, an enhancement of IEF Ey to ~ 10 mV/m, and an increase in solar wind speed to ~ 600 km s^{-1}. The main phase exhibited a two-step development in both interplanetary and geomagnetic parameters. During the post-storm recovery phase (18–19 March), the Dst index gradually

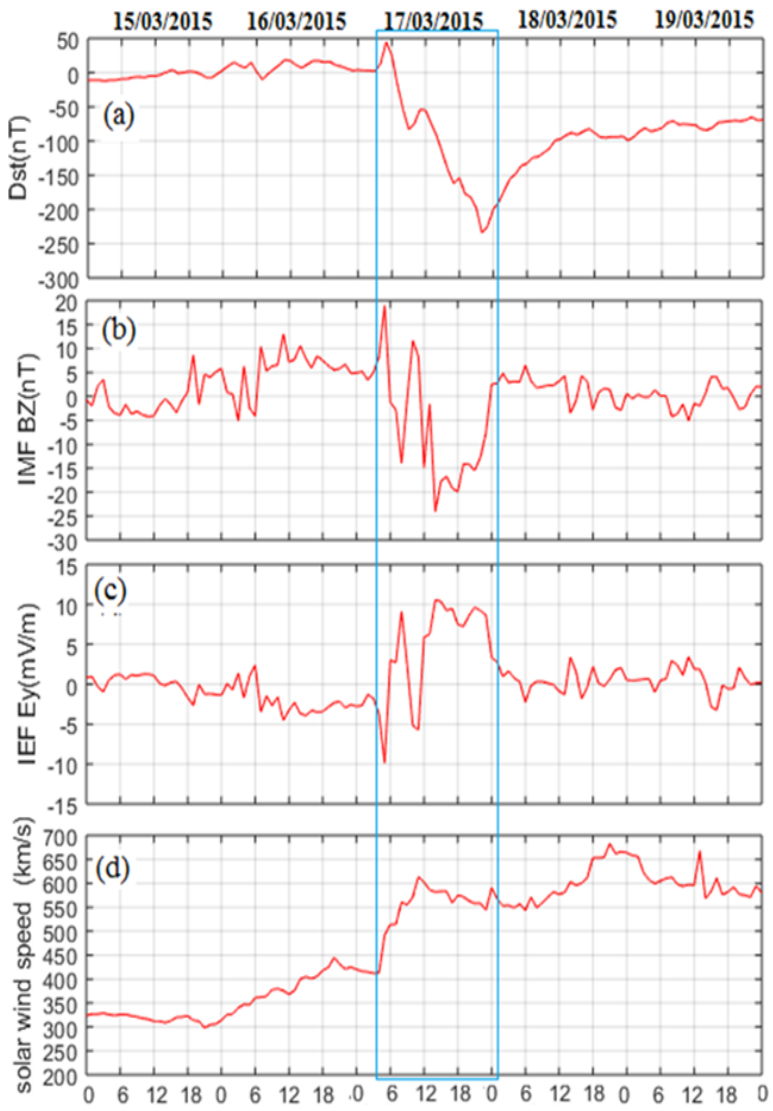

Fig. 1: Variations of (a) Dst, (b) IMF Bz, (c) IEF Ey and (d) solar wind speed between 15th and 19th March 2015.

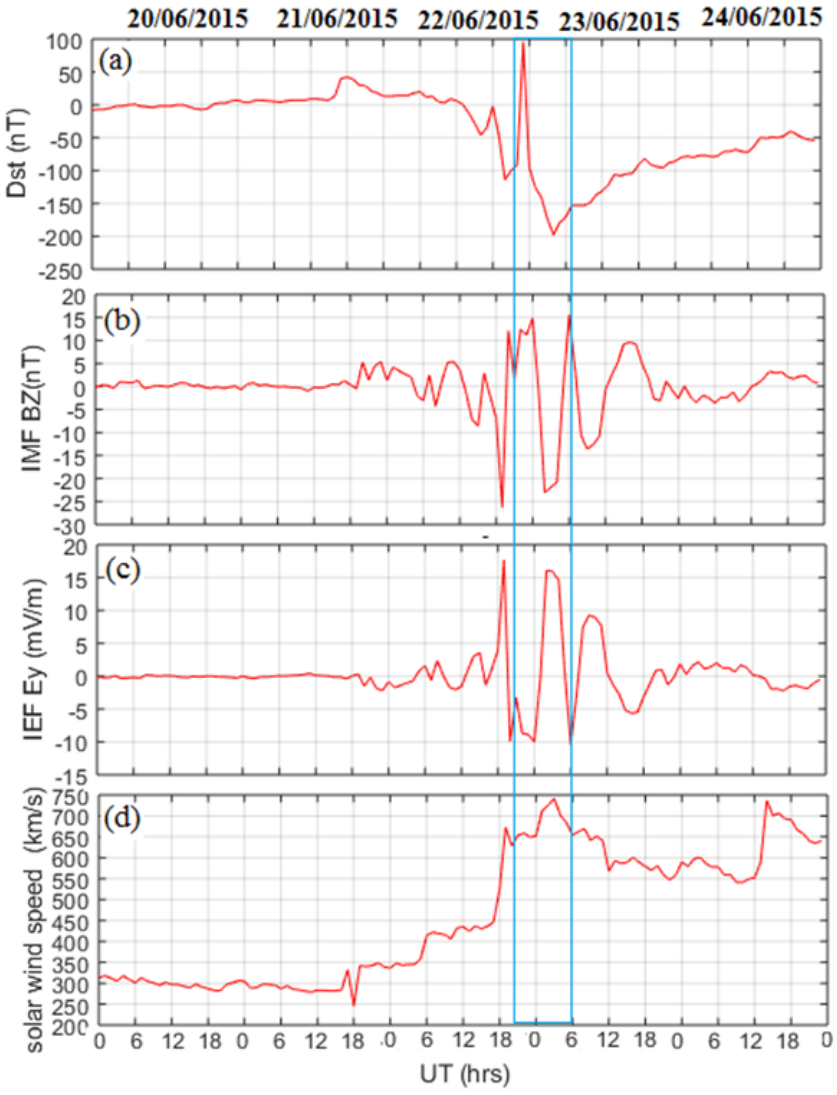

Fig. 2: Variations of (a) Dst, (b) IMF Bz, (c) IEF Ey and (d) solar wind speed between 20th and 24th June 2015.

returned toward pre-storm values, while IMF Bz oscillated northward and southward with reduced magnitudes, indicating the gradual relaxation of the magnetosphere.

The 22 June 2015 storm also displayed a clear multi-step response. At $\sim 21{:}00$ UT on 22nd June, the IMF Bz turned strongly southward to -22 nT, accompanied by an increase in IEF Ey to ~ 15 mV m^{-1} and a solar wind speed enhancement to ~ 700 km s^{-1}. The Dst index reached its minimum during this interval, indicating the storm's main phase. The recovery phase progressed gradually, with Dst rising to −50 nT by 24 June. At this stage, IMF Bz had weakened to $\sim +1$ nT, IEF Ey decreased to ~ 2 mV m^{-1}, and solar wind speed also declined, as shown in Fig. 2(a-d).

The enhanced solar wind speeds observed during the storm intervals are consistent with increased solar activity, particularly coronal mass ejections (CMEs) and solar flares.

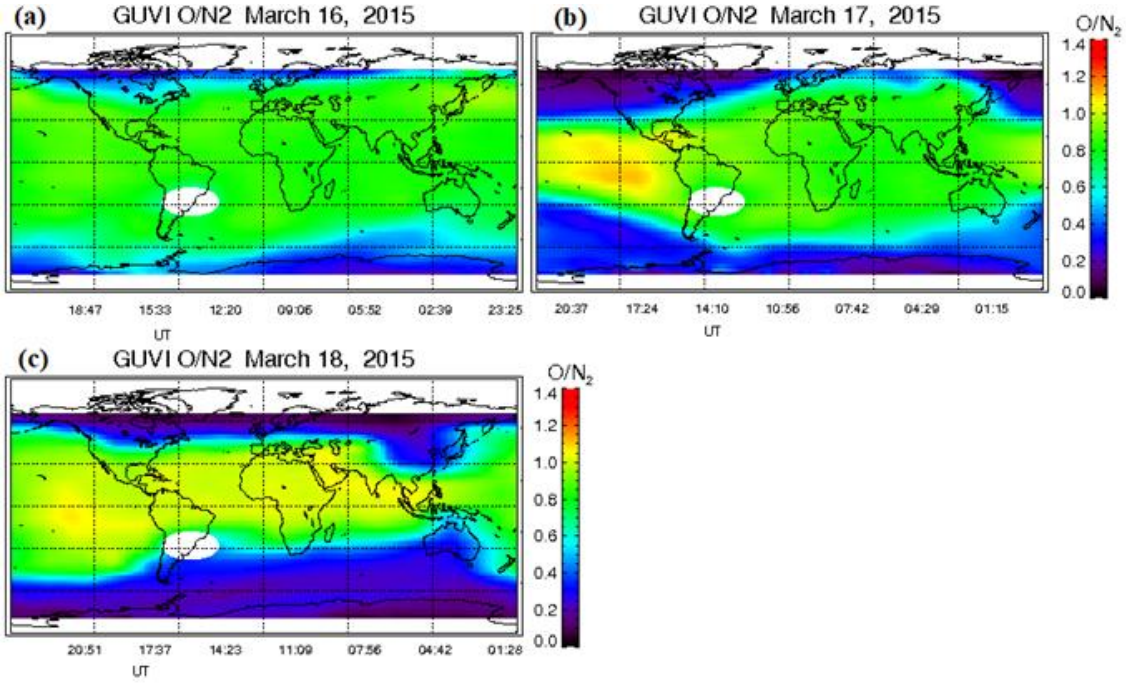

Fig. 3: Global O/N2 map ratio on 16, 17 and 18 March 2015.

These phenomena release large quantities of energetic charged particles, which propagate through the heliosphere as high-speed solar wind streams, ultimately driving intense geomagnetic disturbances.

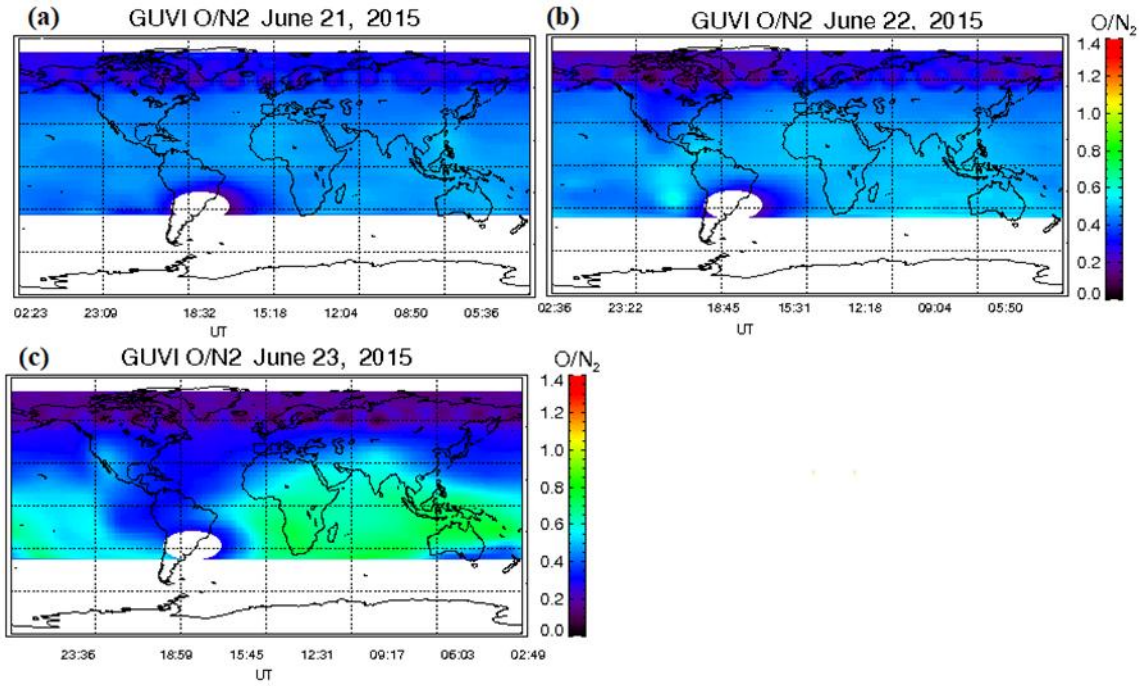

Fig. 4: Global O/N2 map ratio on 21, 22 and 23 June 2015.

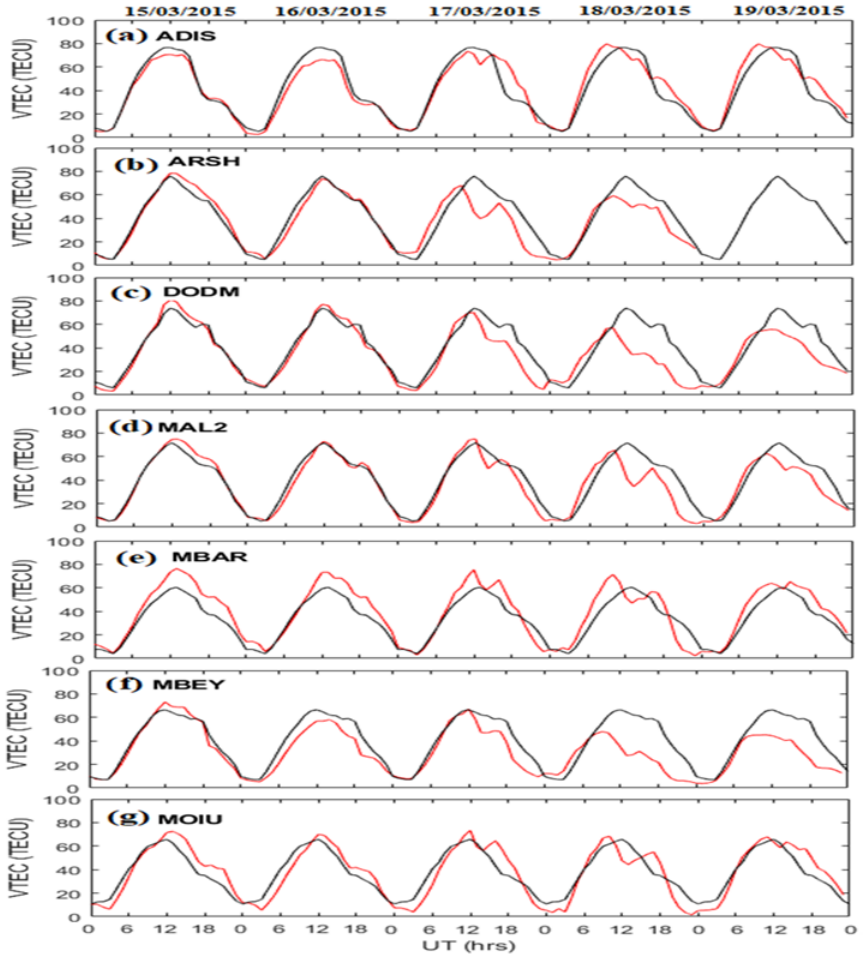

Fig. 5: VTEC variations over (a) ADIS, (b) ARSH, (c) DODM, (d) MAL2, (e) MBAR, (f) MBEY and (g) MOIU between 15th and 19th March 2015.

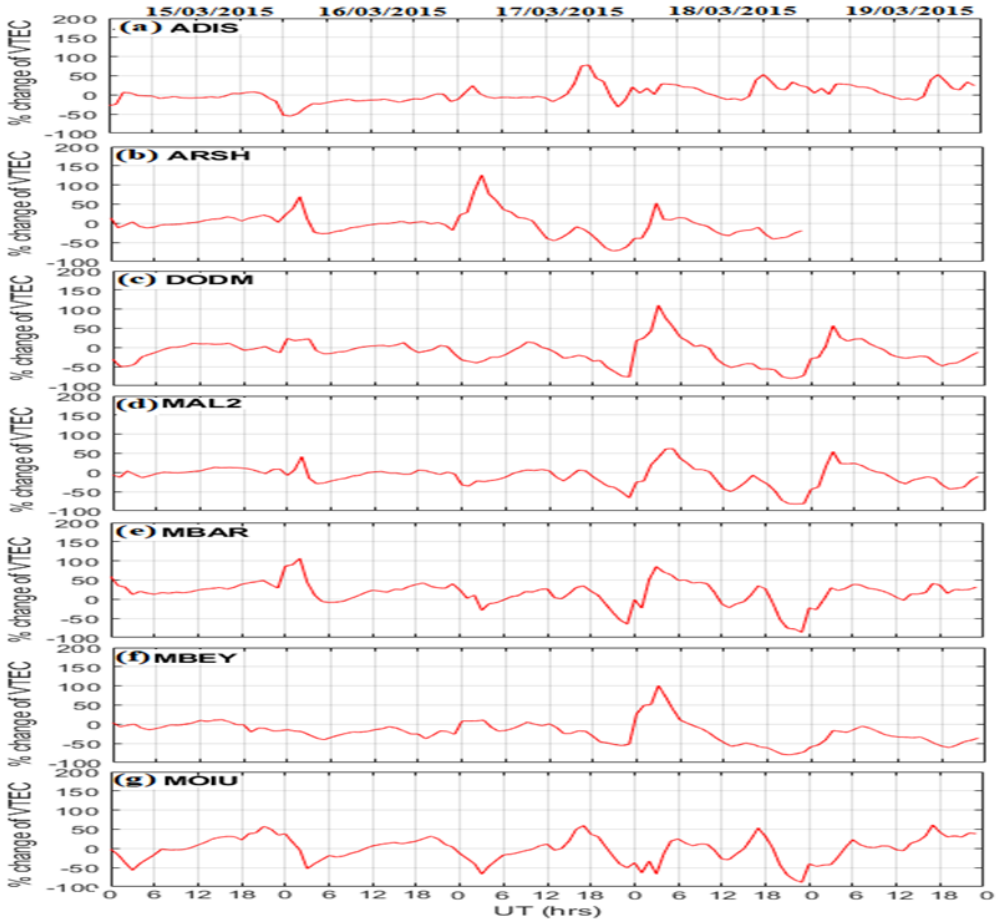

Fig. 6: % change in VTEC over (a) ADIS, (b) ARSH, (c) DODM, (d) MAL2, (e) MBAR,(f) MBEY and (g) MOIU, between 15 and 19 March 2015.

3.2. Global O/N2 map ratio

Fig. 3 and Fig. 4 show the global O/N2 map ratio on 16, 17, and 18 March 2015 and 21, 22, and 23 June 2015, respectively.

In Fig. 3(a), it is observed that on 16 March 2015, before the storm, the global O/N_2 ratio was relatively high. Values approached ~ 1.0 across the equatorial and mid-latitude regions, while the high-latitude regions exhibited lower ratios of ~ 0.5, with localized areas in the Southern Hemisphere dropping below 0.2. On 17 March 2015, during the main phase of the storm (Fig. 3b), the O/N_2 ratio exhibited a marked depletion at high latitudes, with values falling below 0.2 in both hemispheres. This depletion reflects a storm-time enhancement in molecular nitrogen relative to atomic oxygen, a compositional change that increases ionospheric recombination rates and contributes to negative storm effects at mid- and low-latitudes. In contrast, the equatorial and mid-latitude regions maintained relatively elevated ratios of ~ 0.9, indicating enhanced atomic oxygen relative to molecular nitrogen. By 18 March 2015, corresponding to the recovery phase (Fig. 3c), the O/N_2 ratio in the high-latitude regions further decreased to < 0.2, particularly across the Southern Hemisphere. Meanwhile, in the equatorial sector, especially over East Africa, the ratio increased to ~ 1.0, reflecting a compositional recovery in the thermosphere.

For the 22 June 2015 storm, the pre-storm day of 21st June (Fig. 4a) was characterized by globally reduced O/N_2 values, remaining below 0.2 throughout most regions. On 22 June 2015, coinciding with the storm's main phase (Figure 4b), the O/N_2 ratio increased slightly along the equatorial belt, reaching values < 0.6, while the high-latitude regions persisted with very low values (~ 0.2). During the recovery phase on 23rd June 2015 (Fig. 4c), a marked increase in O/N_2 ratio was observed in the equatorial region (~ 0.8), whereas the high latitudes continued to show depressed values (< 0.2). Overall, as illustrated in Fig. 6, the 22nd June 2015 storm was consistently associated with depleted O/N_2 ratios at high latitudes during its initial, main, and recovery phases.

3.3. Variation of VTEC

Fig. 5 and Fig. 6 show VTEC variations and % change in VTEC over (a) ADIS, (b) ARSH, (c) DODM, (d) MAL2, (e) MBAR, (f) MBEY, and (g) MOIU, respectively.

Fig. 5 illustrates the diurnal variation of VTEC across the studied stations. A general trend was observed, where low VTEC values occurred between 00:00 UT and 04:00 UT, followed by a rise to maximum values around local noon ($\sim 12{:}00$ UT), attributed to enhanced photoionization. Afterward, VTEC decreased during the post-sunset hours. Around 18:00 UT, signatures of both TEC depletion and enhancement were evident, which are attributed to the Pre-Reversal Enhancement (PRE) of the eastward electric field. On 15th March, Mbarara and Arusha recorded the highest VTEC values, reaching ~ 80 TECU, while Mbeya reached ~ 70 TECU at approximately 12:00 UT. On 16 March, the peak VTEC values were ~ 75 TECU at Arusha and Dodoma around 12:30 UT. During the storm day (17 March), both the initial and main phases were characterized by significant increases in peak VTEC across all stations. The most pronounced enhancement occurred at Addis Ababa, where VTEC increased by ~ 10 TECU compared to the previous day's maximum of 68 TECU. As shown in Fig. 4, storm-time TEC enhancements were observed at all stations, with Dodoma and Mbeya recording $\sim 100\%$ increases around 03:00 UT, while Addis Ababa and Malindi showed smaller increases of $\sim 50\%$. The variation in enhancement times among the stations indicates that the geomagnetic storm impacted the East African region with distinct local-time dependencies.

During the recovery phase (18–19 March 2015), most stations (Arusha, Dodoma, Malindi, Mbarara, and Mbeya) recorded lower VTEC values. A pronounced decrease was noted at Mbeya, where maximum VTEC dropped from ~ 60 TECU on 17 March to ~ 50 TECU on 18 March and further to ~ 40 TECU on 19 March. Dodoma showed a similar negative storm effect, with maxima falling to ~50 TECU. In contrast, Addis Ababa maintained relatively stable peak VTEC values (~ 70 TECU) throughout the storm period. These decreases are consistent with a negative ionospheric storm response, primarily linked to changes in the thermospheric composition and dynamics. Specifically, storm-time upwelling and heating enhance molecular nitrogen relative to atomic oxygen (lowering the O/N_2 ratio), thereby increasing recombination and reducing plasma density (Huang et al., 2005). This is corroborated by the O/N_2 depletion observed in Fig. 3(c) over high latitudes, which aligns with the negative TEC responses during recovery.

Furthermore, localized variability was evident: while Mbeya and Dodoma showed strong depletion, stations such as Eldoret and Mbarara exhibited partial recovery in TEC during the same period. These regional differences highlight the spatially heterogeneous response of the ionosphere to geomagnetic storms. The midday TEC enhancements observed at some stations may also be attributed to storm-driven neutral wind effects that redistribute plasma along magnetic field lines, consistent with earlier reports (Huang et al., 2005). These results align with previous studies (Fuller-Rowell et al., 1994; Kumar & Singh, 2010; Astafyeva et al., 2022), which demonstrated that solar wind–magnetosphere energy coupling enhances ring currents and electric fields, thereby modifying ionospheric TEC. The observed suppression of plasma irregularities during the storm's main phase also supports earlier findings by Watson et al. (2011), who noted that disturbed electrodynamics and neutral winds during intense storms can suppress irregularity growth.

Fig. 7 and Fig. 8 show the VTEC variations and % change in VTEC over ADIS, (b) ARSH, (c) MAL2, (d) MBEY, and (e) MOIU, between 20 and 24 June 2015. respectively. Fig. 7 presents the diurnal variation of VTEC for the period 20–24 June 2015. On 20 June 2015, all stations attained their daily maximum VTEC around 12:00 UT.

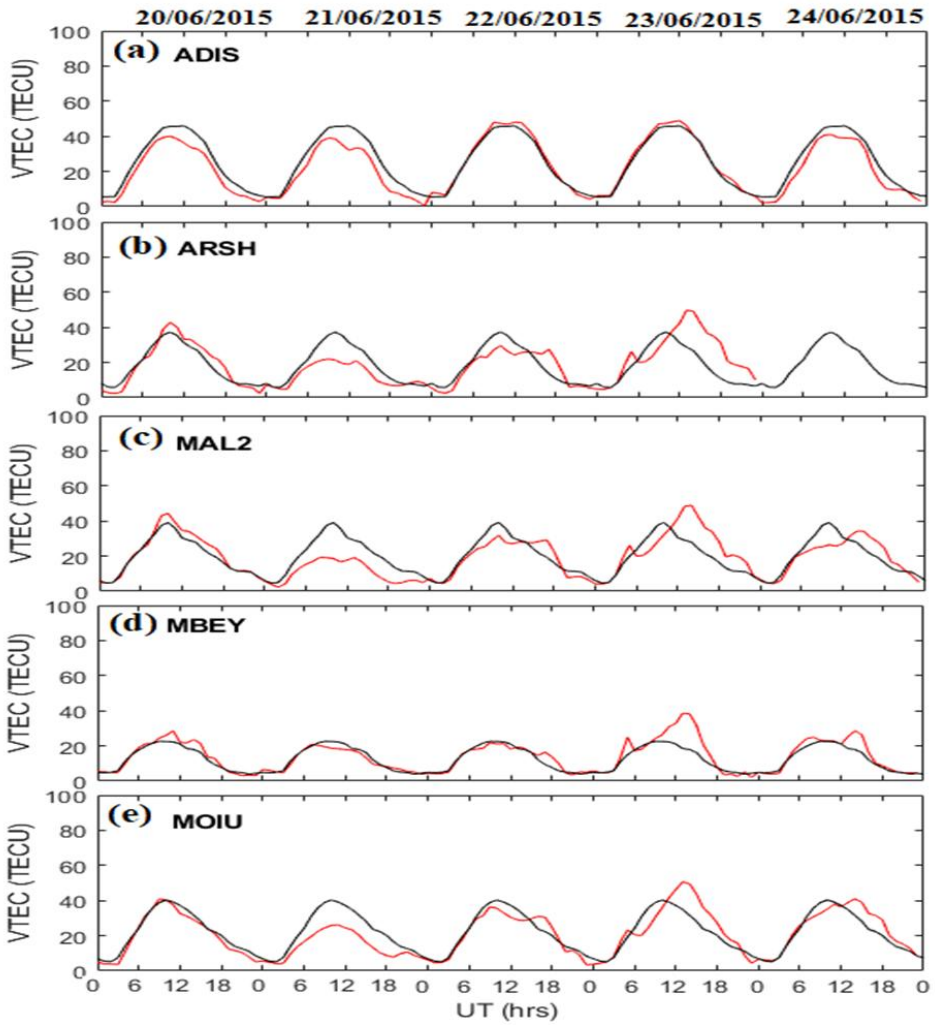

Fig. 7: VTEC variations over (a) ADIS, (b) ARSH, (c) MAL2, (d) MBEY and (e) MOIU, between 20th and 24th June 2015.

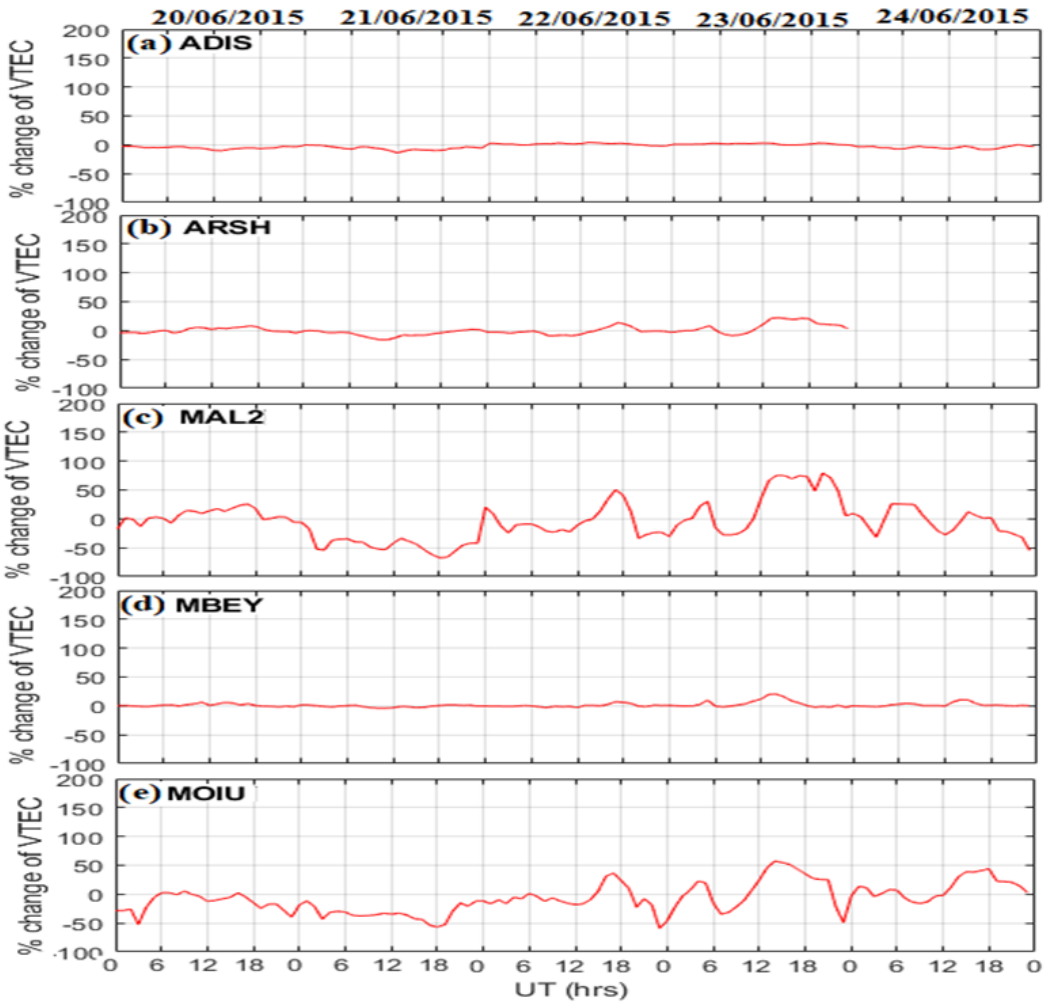

Fig. 8: % change of VTEC variations over ADIS, (b) ARSH, (c) MAL2, (d) MBEY and (e) MOIU, between 20th and 24th June 2015.

consistent with enhanced photoionization near local noon.

On 20 June 2015, all stations attained their daily maximum VTEC around 12:00 UT. Addis Ababa recorded the highest value ($\sim$50 TECU), while Mbeya registered the lowest ($\sim$30 TECU). On 21 June 2015, there was a general decrease in peak VTEC across most stations, except Addis Ababa, which maintained stable values. The largest reduction was observed over Mbeya, where the maximum VTEC decreased by $\sim$10 TECU compared to the previous day. On 22 June 2015, which corresponded to the storm day, the VTEC response varied across stations. Addis Ababa recorded the highest maximum ($\sim$40 TECU), while Mbeya registered the lowest ($\sim$20 TECU). The suppressed VTEC levels across most stations were associated with the prompt penetration of high-latitude electric fields (PPEFs). These electrodynamic disturbances, which rapidly propagate to low latitudes during geomagnetic storms, uplift plasma along magnetic field lines and redistribute it, producing both enhancements and depletions in TEC. Similar storm-time responses attributed to PPEFs have been documented by Aol et al. (2019), who reported positive storm-time TEC effects over the African sector.

During the recovery phase (23 June 2015), VTEC values increased across all stations. Addis Ababa recorded the highest maximum ($\sim$50 TECU), whereas Mbeya had the lowest ($\sim$40 TECU). By 24 June 2015, the VTEC values decreased again across all stations, with Mbeya recording the lowest maximum ($\sim$30 TECU). These reductions were associated with storm-driven changes in the neutral thermospheric composition. Specifically, as illustrated in Fig. 8, there was a notable increase in the O/N_2 ratio over the equatorial region on 23 June, reflecting compositional recovery after the storm.

The observed variations in VTEC are consistent with previous studies. For example, Amaechi et al. (2018) reported that changes in neutral composition during geomagnetic storms, particularly reductions in the O/N_2 ratio, strongly control ionospheric plasma density and TEC. In this study, the low O/N_2 ratios during the storm phase explain the suppressed VTEC values, while the subsequent recovery in O/N_2 ratios on 23 June corresponds to the restoration of TEC across the East African stations.

4. Conclusion

The investigation of the geomagnetic storms of 17 March 2015 and 22 June 2015 demonstrates that intense geomagnetic activity exerts a pronounced influence on the ionosphere over the East African sector. The 17 March 2015 event was predominantly characterized by negative storm effects during its initial and main phases, manifested as TEC depletion. This response was likely driven by storm-induced downward E×B drifts and concurrent reductions in the O/N_2 ratio, which enhanced ionospheric recombination. In contrast, the 22 June 2015 storm exhibited positive storm effects during its recovery phase, with enhanced TEC across multiple stations. These enhancements were attributed to the prompt penetration of high-latitude electric fields (PPEFs) and the strengthening of the Equatorial Ionization Anomaly (EIA).

The results further indicate that local time and seasonal conditions modulate the ionospheric response to geomagnetic storms. The 17 March event, which occurred during the equinox, produced higher TEC values across all stations compared to the 22 June storm, which took place during the solstice. This seasonal dependence aligns with prior studies, highlighting the complex interplay between solar wind–magnetosphere coupling, storm-time electric fields, thermospheric composition changes, and equatorial electrodynamics in shaping ionospheric variability.

These findings provide critical insights for understanding and modeling storm-time ionospheric dynamics, particularly over the equatorial East African region, where the ionosphere is highly sensitive to space weather disturbances. Such knowledge is essential for improving the reliability of GNSS-based applications and for mitigating the adverse impacts of geomagnetic storms on communication and navigation systems.

Acknowledgements

The authors thank the University of NAVSTAR Consortium: http://unavco.org/data/gps-gnssdata/ for the GNSS data and Prof Gopi Seemala for the GPS-TEC analysis software.

The authors express gratitude to Masinde Muliro University of Science and Technology (MMUST) for providing a library and internet, which made the research work easier.

References

Abdu, M. A; Khelerani, Alam; Batista, E; de-paula, E. R; Fritts, D. C; Sobral, J H;. (2009). Gravity wave initiation of equatorial spread F/plasma bubble irregularities based on observational data from the SpreadFEx campaign. *Annals of Geophysis*, 27(7), 2607-2622.

Adewale, A. O., Oyeyemi, E. O., Adeloye, A. B., Mitchell, C. N., & Cilliers, P. J. (2012). A Study of L-Band scintillations and total electron content at an Equitorial station Lagos Nigeria. *Radio science*, 47.

Amaechi, P. O., Oyeyemi, E. O., & Akala, A. O. (2018). Geomagnetic storm effects on the occurrences of ionospheric irregularities over the African equatorial/Low-lattitude region. *Advances in Space Research*.

Aol, Sharon; Mungufeni, Patrick; Jurua, Edward. (2019). Effects of space weather on the ionosphere: A case study of geomagnetic storms during 17-28 February 2014. *Indian Journal of Radio and space physics*, 48, 26-37.

Arikan, F; Nayir, H; Sezen, U; Arikan, O;. (2008). Estimation of single interfrequency receiver bias using GPS-TEC. *Radio Science*, 43.

Astafyeva, E; Yasyukukevich, Y. V; Maletckii, B; Oinats, A;

Vesnin, A; Yasyukevich, A. S; Syrovatskii, S; Guendouz, N. (2022). Ionospheric Disturbances and Irregularities During the 25–26 August 2018 Geomagnetic Storm. Journal *of Geophysical Research* : Space Physics, 127(1).

Carmo, C. S., Dai, L., Denardini, C. M., Figueiredo, C. A., Wrasse, C. M., & Resende, L. C. (2023). Equatorial plasma bubbles features over the Brazilian sector according to the solar cycle and geomagnetic activity level. *Frontiers in Astronomy and space Sciences*, 10(1252511).

Carmo, C. S; Dai, L.; Wrasse, C. M; Barros, D; Takahashi, H; Figueiredo, C. A; Wang, C; Li, H; Liu, Z. (2024). Ionospheric Response to the Extreme 2024 Mother's Day Geomagnetic Storm Over the Latin American Sector. *Advancing Earth and Space sciences*, 22(e2024SW004054).

Chukwuma, Moses Anoruo; Babatunde, Rabiu; Daniel, Okoh; Fransica, Nneka, Okeke; Kingsley, Chukwudi Okpala. (2022). Irregularities in the African ionoshere associated anomalies observed during high solar activity levels. *Frontiers in Astronomy and space sciences*.

Feng, J., Zhou, Y., Zhou, Y., Gao, S., Zhou, C., Tang, Q., et al. (2021). Ionospheric response to the 17 March and 22 June 2015 geomagnetic storms over Wuhan Region using GNSS- based tomographic technigue. *Advances In Space Research*, 67, 111-121.

Fuller-Rowell, T. J., Codrescu, M. V., Roble, R. G., & Richmond, A. D. (1994). How does the thermosphere and ionosphere react to a geomagnetic storm? Advances in Space Research, 14(1), 33-35.

Habyarimana, V., Habarulema, J., & Dugassa, T. (2023). Analysis of ionospheric storm-time effects over the East African sector during the 17 March 2013 and 2015 geomagnetic storms. *Earth, Planets and Space*.

Huang, C., Foster, J. C., Goncherenko, L. P., Erickson, P. J., Rideout, W., & Coster, A. J. (2005). A strong postive phase of ionosphere storms observed by the Millstone Hill incoherent scatter radar and global GPS network. *J.Geophysics Res*, 110(A06303).

Kintner, P. M; Ledvina, B. M; de-Paula, E. R;. (2007). GPS and ionospheric scintillations. *Space Weather*, 5(s09003).

Klobuchar, J. A. (1987, May). Ionospheric Time-Delay Algorithm for Single-Frequency GPS. *IEEE Transactions on Aerospace and Electronic systems*, AES-23(3), 325-331.

Kumar, S., & Singh, A. K. (2010). The effect of geomagnetic storm on GPS derived TEC at varansi India. *J.Physics.cont*, 208(1).

Lissa, D; Srinivasu, V. K; Prasad, D. S; Niranjan, K;. (2020). Ionospheric response to the 26 August 2018 geomagnetic storm using GPS-TEC observations along 80° E and 120° E longitudes in the Asian sector. *Advances in Space Research*, 66, 1427-1440.

Muniafu, W., Uluma, E., Lemotey, S. O., Nguessan, K., Bankole, F. J., Uga, C. I., et al. (2024). Ionospheric Total Electron Content Response to the Intense Geomagnetic Storm of 10th -11th May 2024 over Low, Mid and High Latitude Regions. *Asian Journal of Research and Reviews in Physics*, 8(4), 19-36.

Ngwira, C., Seemela, G., & Habarulema, J. (2013). Simultaneous observations of ionospheric irregularities in the African low-latitude region. *Journal of Atmospheric and solar- Terrestrial Physics*, 97, 50-57.

Olwendo, J. O., Yamazaki, Y., Cilliers, P., Baki, P., Ngwira, C. M., & Mito, C. (2015). A Study on the response of the Equatorial Ionization Anomaly over the East Africa sector during the geomagnetic storm of November 13, 2012. Adv. *Space Res*.

Ondede, George, Ochieng; Rabiu, A. B; Okoh, Daniel; Baki, Paul; Olwendo, Joseph; Shiokawa, Kazuo; Otsuka, Yuichi;. (2022). Relationship between geomagnetic storms occurance of ionospheric irreguralities in the west sctor of Africa during the peak of the 24th solar cycle. *Frontiers in Astronomy and space sciences*.

Pokharia , M; Prasad, I; Bhoj, C; Mathpal, C;. (2018). A study of geomagnetic storms and solar and Interplanetary parameters for solar cycles 22 and 24. *Solar Physics*, 293(126).

Sardon , E; Rius, A; Zarrao, N. (1994). Estimation of the transmitter and receiver differential biases and the ionospheric total electron content from Global positioning system observations. *Radio science*, 29, 577-586.

Sardon, Esther; Zarraoa, Nester. (1997). Estimation of total electron content using GPS data: How stable are differential satellite and receiver instrumental biases? *Radio science*, 32(5), 1899-1910.

Seemala, G. K; Valladares, C. E. (2011). Statistics of TEC depletions observed over the South American continent for the year 2008. Radio Science, 46(RS5019).

Tilahun, A.M.; Uluma, E.; Ejigu, Y.G. Variation in Total Electron Content During a Severe Geomagnetic Storm, 23–24 April 2023. *Atmosphere* 2025, *16*, 676. https://doi.org/10.3390/atmos16060676

Uluma, E., Ndinya, B., & Omondi, G. (2019). Variability of VTEC Gradient and TEC Rate Index Over Kisumu, Kenya During Selected Quiat and Storm Days of 2013 and 2014. *American Journal of Astronomy and Astrophysics*, 7(4), 67-72.

Uluma E, Lomotey S O, Bankole F J, Nguessan K, Muniafu W, Mefe M, Uga C I, Omondi G, Were A and Ndinya B (2025). Investigation of ionospheric irregularities during the severe geomagnetic storm of 10–11 May 2024. *Indian Journal of Physics*. https://doi.org/10.1007/s12648-025-03734-6.

Watson, C; Jayachandran, P. T; MacDougall, J. W; Terkildsen, M;. (2011). Ionospheric responses and scintillation during geomagnetic storms. Journal of Geophysical Research: *Space Physics*, 116(A12)(A12318).